Atmos. Chem. Phys. Discuss., 13, 17479–17517, 2013
www.atmos-chem-phys-discuss.net/13/17479/2013/
doi:10.5194/acpd-13-17479-2013

Atmospheric Chemistry and Physics Discussions

Inverse modeling of Texas NO_x emissions using space-based and ground-based NO_2 observations

W. Tang[1], D. Cohan[1], L. N. Lamsal[2,3], X. Xiao[1], and W. Zhou[1]

[1]Department of Civil and Environmental Engineering, Rice University, 6100 Main Street MS 519, Houston, TX 77005, USA
[2]NASA Goddard Space Flight Center, Greenbelt, MD, USA
[3]Goddard Earth Sciences Technology & Research, Universities Space Research Association, Columbia, MD, USA

Received: 21 June 2013 – Accepted: 25 June 2013 – Published: 2 July 2013

Correspondence to: W. Tang (wei.tang@rice.edu)

Published by Copernicus Publications on behalf of the European Geosciences Union.

Abstract

Inverse modeling of nitrogen oxide (NO_x) emissions using satellite-based NO_2 observations has become more prevalent in recent years, but has rarely been applied to regulatory modeling at regional scales. In this study, OMI satellite observations of NO_2 column densities are used to conduct inverse modeling of NO_x emission inventories for two Texas State Implementation Plan (SIP) modeling episodes. Addition of lightning, aircraft, and soil NO_x emissions to the regulatory inventory narrowed but did not close the gap between modeled and satellite observed NO_2 over rural regions. Satellite-based top-down emission inventories are created with the regional Comprehensive Air Quality Model with extensions (CAMx) using two techniques: the direct scaling method and discrete Kalman filter (DKF) with Decoupled Direct Method (DDM) sensitivity analysis. The simulations with satellite-inverted inventories are compared to the modeling results using the a priori inventory as well as an inventory created by a ground-level NO_2 based DKF inversion. The DKF inversions yield conflicting results: the satellite-based inversion scales up the a priori NO_x emissions in most regions by factors of 1.02 to 1.84, leading to 3–55 % increase in modeled NO_2 column densities and 1–7 ppb increase in ground 8 h ozone concentrations, while the ground-based inversion indicates the a priori NO_x emissions should be scaled by factors of 0.34 to 0.57 in each region. However, none of the inversions improve the model performance in simulating aircraft-observed NO_2 or ground-level ozone (O_3) concentrations.

1 Introduction

Nitrogen oxides (NO_x = NO + NO_2) in the troposphere are primary air pollutants, emitted from both anthropogenic sources like fossil-fuel combustion and biomass burning, and natural sources such as soil microbial processes and lightning. NO_x also acts as a precursor of a secondary air pollutant, tropospheric O_3, when it reacts with the oxidation products of volatile organic compounds (VOCs) in the presence of sunlight. Ox-

ACPD
13, 17479–17517, 2013

idation with hydroxyl (OH) radical is the dominant sink of NO_x, leading to atmospheric nitric acid (HNO_3) formation. The atmospheric lifetime of tropospheric NO_x varies from a few hours in summer to a couple of days in winter (Seinfeld and Pandis, 2006).

NO_x emission inventories used in air quality modeling are typically developed by a bottom-up approach based on estimated activity rates and emission factors for each category. Due to inaccuracies in determining these rates and factors, the uncertainty in NO_x emission inventories has been suggested to be as high as a factor of two and classified as one of the top uncertainties in ozone simulations and sensitivity analysis (Hanna et al., 2001; Xiao et al., 2010).

Inverse modeling techniques can be used with atmospheric models to estimate model variables that may not be directly measurable (Gilliland and Abbitt, 2001). Inverse modeling generates an optimized "top-down" NO_x emission inventory for air quality models by minimizing the difference between observed and modeled NO_2 concentrations, providing an opportunity to identify possible biases in the bottom-up NO_x emission inventory (Napelenok et al., 2008). However, as uncertainties may also associate with the measurement data and the inverse methods themselves, inverse modeling has its own limitations. Hence, it is valuable to compare both bottom-up and top-down NO_x emission inventories in order to improve the understanding of NO_x emissions.

Several inverse modeling studies have used surface NO_2 measurements (Mendoza-Dominguez and Russell, 2000; Quélo et al., 2005; Pison et al., 2007) or aircraft NO_2 measurements (Brioude et al., 2011) to constrain NO_x emissions. Compared to ground and aircraft measurements, satellite-based observations generate greater spatial coverage of NO_2. Studies on combining satellite NO_2 measurements with inverse modeling techniques to create the top-down NO_x emission inventories also have been conducted recently in both global scale (Martin et al., 2003; Müller and Stavrakou, 2005; Jaeglé et al., 2005; Lin et al., 2010) and regional scale modeling (Konovalov et al., 2006, 2008; Deguillaume et al., 2007; Napelenok et al., 2008; Kurokawa et al., 2009; Zhao and Wang, 2009; Chai et al., 2009).

ACPD
13, 17479–17517, 2013

Discrete Kalman filter (DKF) (Prinn, 2000) is an inverse modeling method that solves the inverse problem iteratively, and can be applied to the cases with linear or weakly non-linear relationships between emissions and pollutants. It has been used in several studies to constrain emissions of carbon monoxide (Mulholland and Seinfeld, 1995), chloroflourocarbons (Haas-Laursen et al., 1996), isoprene (Chang et al., 1996) and ammonia (Gilliland et al., 2003). Most recently, Napelenok et al. (2008) applied the DKF method to the regional Community Multiscale Air Quality (CMAQ) model, generating a top-down NO_x emission inventory for the southeastern United States using Scanning Imaging Absorption Spectrometer for Atmospheric Chartography (SCIAMCHY) (Bovensmann et al., 1999) satellite NO_2 data.

Despite the growing number of scientific studies conducting satellite-based inversions of NO_x emissions, the applicability of these methods to state-level regulatory attainment modeling has not been widely explored. In this work, the DKF method introduced by Napelenok et al. (2008) is applied with finer resolution satellite NO_2 data now available from the Ozone Monitoring Instrument (OMI) as well as ground-level NO_2 observations, to constrain NO_x emissions for actual regulatory modeling episode in Texas. Lightning and aircraft NO_x emissions are added to the base case NO_x emission inventory to address the bias noted by Napelenok et al. (2008) of regional models underestimating upper tropospheric NO_x. The DKF inverted a posteriori emissions are compared to the base case emissions, the a priori emissions and a posteriori emissions derived by the inversion method of Martin et al. (2003).

2 Methodology

2.1 Model inputs and configurations

Base case model inputs were taken from episodes developed by the Texas Commission on Environmental Quality (TCEQ) for Texas ozone attainment planning. CAMx version 5.3 (ENVIRON, 2010) was used in this study to simulate two modeling episodes

ACPD
13, 17479–17517, 2013

in 2006 with high ozone concentrations in the Dallas–Fort Worth (DFW) region, from 31 May to 1 July, and in the Houston–Galveston–Brazoria (HGB) region, from 13 August to 15 September (Fig. 1). The NCAR/Penn State (National Center for Atmospheric Research/Pennsylvania State University) Mesoscale Model, Version 5, release 3.7.3 (MM5v.3.7.3) (Grell et al., 1994), conducted with the Eta-PBL scheme, was used to generate the meteorological fields with 43 vertical layers. The preprocessor MM5CAMx was used to convert MM5 outputs into CAMx-ready meteorology inputs. The vertical configuration of CAMx modeling consists of 17 vertical layers for the August–September modeling episode, whereas 28 vertical layers were used for the June modeling episode. Modeling was conducted with the Carbon Bond version 2005 (CB-05) chemical mechanism, PPM advection scheme, and K-theory vertical diffusion scheme (TCEQ, 2010, 2011). Boundary conditions for the 36 km eastern US domain were generated by the Model for Ozone and Related Chemical Tracers (MOZART) global model (ENVIRON, 2008).

2.2 Emission inventory

Base case emission inventories were provided by TCEQ. The point source emissions were from the State of Texas Air Reporting System (STARS) database which collects emission information from approximately 2000 point sources annually, and the EPA's acid rain database (ARD) which contains emissions from electric generating units (EGUs). The on-road mobile emission inventory was generated by Motor Vehicle Emission Simulator 2010a (MOVES2010a), and the non-road mobile inventory was developed by National Mobile Inventory Model (NMIM) and the Texas NONROAD (TexN) mobile source model. The area source inventory was projected by the EPA Economic Growth Analysis System (EGAS) model based on 2005 emissions from the Texas Air Emissions Repository (TexAER) database. The Emission Processing System, version 3 (EPS3) (ENVIRON, 2007) was used for processing the point, mobile, and area emissions to the model-ready format (TCEQ, 2010, 2011). Biogenic emissions were generated by the Global Biosphere Emissions and Interactions System (GloBEIS) biogenics

ACPD
13, 17479–17517, 2013

emissions model, version 3.1 (Yarwood et al., 1999), with soil NO_x emissions estimated by the Yienger and Levy method (Yienger and Levy, 1995).

Lightning and aircraft NO_x emissions in the upper troposphere were missing in the base case emission inventories and should be added before conducting inversions. In this study, lightning NO emissions were developed based on National Lightning Detection Network (NLDN) data obtained from Vaisala Inc., following the approach of Kaynak et al. (2008). Intra-cloud lightning flashes were treated as three times of cloud-to-ground lightning flashes with 500 mol NO emission per flash. Lightning NO was placed into the model to match the time and location of NLDN flashes, and then distributed vertically based on the profile obtained from the mean April to September 2003–2005 vertical distribution of VHF sources from the Northern Alabama Lightning Mapping Array (Koshak et al., 2004). Global aircraft NO_x emissions of year 2005 in $0.1^\circ \times 0.1^\circ$ resolution were obtained from the Emission Database for Global Atmospheric Research (EDGAR) v4.1 (http://edgar.jrc.ec.europa.eu/datasets_grid_list41.php?v=41&edgar_compound=NOx) and mapped to our modeling domain and placed at 9 km altitude.

2.3 Inversion regions

Five urban areas: Houston–Galveston–Brazoria (HGB), Dallas–Fort Worth (DFW), Beaumont–Port Arthur (BPA), Northeast Texas (NE Texas), and Austin and San Antonio; plus two surrounding rural areas: North Rural area (N rural) and South Rural area (S rural) (Fig. 1) were designed as inversion regions for the DKF inversions of NO_x emissions. The five urban regions are all air quality planning areas included in Texas SIP development (Gonzales and Williamson, 2011). HGB and DFW were classified by US EPA as ozone nonattainment areas for violating the 1997 ozone National Ambient Air Quality Standard (NAAQS) of 84 ppb. BPA was designated as an ozone maintenance area, and NE Texas, Austin and San Antonio were designated as ozone early action compact areas under that standard. However, the recent tightening of the NAAQS to 75 ppb has heightened interest in ozone reduction in all of these regions.

ACPD
13, 17479–17517, 2013

The sensitivities of NO_2 concentrations to boundary conditions and to NO_x emissions from each inversion region and the border region (the area between model boundary and inversion regions) were computed through DDM. The border region minimizes the impacts from boundary conditions on the inversion regions to the level of only 2 %. The DDM sensitivities show that NO_x emissions from each urban region has the most impact on NO_2 concentrations within that region, and has less than 10 % influence on other regions.

2.4 Inversion methods

Two methods are applied for inverse modeling: a direct scaling method introduced by Martin et al. (2003), and the DKF method.

2.4.1 Direct Scaling (DS) inversion method

The DS method applies the ratio between satellite NO_2 observations and modeled NO_2 concentrations to scale the bottom-up NO_x emissions in each grid cell:

$$E_t = E_b \times \frac{\Omega_s}{\Omega_m} \quad (1)$$

where E_t is the top-down NO_x emission rate; E_b is the bottom-up NO_x emission rate; Ω_s and Ω_m are the satellite and modeled NO_2 column densities, respectively.

This method was developed in a global model with coarse grid resolution and assumes that the NO_2 concentration in each model grid will not be affected by the NO_x emitted from surrounding grids. However, in a regional model with relatively small grid size, this assumption may fail, generating a spatial smearing error when NO_x lifetime is longer than the horizontal transport time (Martin et al., 2003; Boersma et al., 2008; Lamsal et al., 2010; Turner et al., 2012). Martin et al. (2003) indicated that the spatial smearing error can be neglected if the grid length is greater than 100 km. Therefore, smoothing kernels (Toenges-Schuller et al., 2006; Boersma et al., 2008; Lamsal et al.,

ACPD
13, 17479–17517, 2013

2010) need to be applied in order to alleviate the spatial smearing error in CAMx by accounting for the emissions from adjacent grid cells in developing the top-down NO_x emissions. The smoothing kernel is defined as

$$\mathbf{K} = \frac{1}{k+8}\begin{pmatrix} 1 & 1 & 1 \\ 1 & k & 1 \\ 1 & 1 & 1 \end{pmatrix} \quad (2)$$

where k is a smoothing parameter, and is determined by applying the smoothing kernel ($\mathbf{K}$) to each grid cell in the bottom-up NO_x emission inventory with different k values until the correlation between smoothed bottom-up NO_x emissions and corresponding CAMx modeled NO_2 column density reaches a maximum. The smoothing kernel ($\mathbf{K}$) is then applied to Eq. (1) to form Eq. (3),

$$E^{\mathrm{t}}_{i,j} = \frac{E^{\mathrm{b}}_{i,j}}{\sum_{n=-1}^{1}\sum_{l=-1}^{1}\mathbf{K}_{l,n}E^{\mathrm{b}}_{i+l,j+n}}\frac{\Omega_{\mathrm{s}}}{\Omega_{\mathrm{m}}} \times E^{\mathrm{b}}_{i,j} \quad (3)$$

where i and j represent column and row in horizontal model grids.

2.4.2 DKF inversion method

The direct scaling inversion approach, as described above, creates spatial smearing errors when applies to the regional models with fine resolution. Meanwhile, it assumes concentrations scale proportionally with emissions; hence, the nonlinearity between NO_2 concentrations and NO_x emissions becomes problematic because NO_x may influence its own lifetime by influencing concentrations of OH radicals (Martin et al., 2003). The DKF inversion (Fig. 2), however, solves the spatial smearing problem by taking the spatial relationship between NO_2 concentrations and NO_x emissions directly from model simulations, and also reduces the non-linearity issue by performing the inversion iteratively.

ACPD
13, 17479–17517, 2013

To constrain NO_x emissions, the DKF inversion includes two processes at each time step: the measurement update (correction) process and the time update (prediction) process (Rodgers, 2000; Welch and Bishop, 2001). In the measurement update process at time step k (Eqs. 4–6), the inversion corrects the predicted NO_x emission ($\mathbf{E}^{-}_{NO_x,k}$) and error covariance ($\mathbf{P}^{-}_{NO_x,k}$) by incorporating the measurement data ($\mathbf{C}^{measured}_{NO_2,k}$) and Kalman Gain ($\mathbf{G}_k$), and then generates the corrected emission ($\hat{\mathbf{E}}_{NO_x,k}$) and error covariance ($\hat{\mathbf{P}}_{NO_x,k}$).

$$\mathbf{G}_k = \mathbf{P}^{-}_{NO_x,k}\mathbf{S}^{T}_{k}\left(\mathbf{S}_k\mathbf{P}^{-}_{NO_x,k}\mathbf{S}^{T}_{k} + \mathbf{R}_k\right)^{-1} \quad (4)$$

$$\hat{\mathbf{E}}_{NO_x,k} = \mathbf{E}^{-}_{NO_x,k} + \mathbf{G}_k\left(\mathbf{C}^{measured}_{NO_2,k} - \mathbf{C}^{modeled}_{NO_2,k}\right) \quad (5)$$

$$\hat{\mathbf{P}}_{NO_x,k} = (\mathbf{I} - \mathbf{G}_k\mathbf{S}_k)\mathbf{P}^{-}_{NO_x,k} \quad (6)$$

S represents the NO_2 sensitivity to NO_x emissions. **R** is the measurement error covariance, and it relates to the uncertainties in OMI and ground NO_2 measurements. In here, the uncertainty for the AQS ground NO_2 measurements was set to 0.15 (US EPA, 2006) and for the NASA standard OMI NO_2, version 2, was set to 0.3 (Bucsela et al., 2013) for all diagonal elements in **R**. The error covariance (**P**) relates to the uncertainty in the NO_x emission inventory, and the uncertainty value of 2.0 (Hanna et al., 2001; Napelenok et al., 2008) was chosen here for all diagonal elements in **P**. To simplify, off-diagonal elements in **R** and **P** were set to zero, because we assume each inversion region is an independent element.

In the time update process at time step k, the inversion process predicts the emission ($\mathbf{E}^{-}_{NO_x,k+1}$) and the error covariance ($\mathbf{P}^{-}_{NO_x,k+1}$) for the measurement update process at time step $k+1$, based on the corrected emission ($\hat{\mathbf{E}}_{NO_x,k}$) and error covariance ($\hat{\mathbf{P}}_{NO_x,k}$)

ACPD
13, 17479–17517, 2013

from the measurement update process at time step k (Eqs. 7, 8).

$$\mathbf{E}^{-}_{\mathrm{NO_x},k+1} = \mathbf{M}_k \widehat{\mathbf{E}}_{\mathrm{NO_x},k} + \boldsymbol{\varepsilon}_k \tag{7}$$

$$\mathbf{P}^{-}_{\mathrm{NO_x},k+1} = \mathbf{M}_k \widehat{\mathbf{P}}_{\mathrm{NO_x},k} \mathbf{M}_k^T + \mathbf{Q}_k \tag{8}$$

M represents a transition matrix; $\boldsymbol{\varepsilon}$ and **Q** are process errors which relate to errors in modeling processes, and are difficult to estimate. Since we assume the bias between modeled and measured NO_2 is mostly from errors in NO_x emissions (Prinn, 2000; Napelenok et al., 2008), $\boldsymbol{\varepsilon}$ and **Q** were set to zero.

CAMx-DDM (Koo et al., 2007) calculates a semi-normalized NO_2 sensitivity to NO_x emissions (unitless), as shown in Eq. (9), replacing sensitivity elements in **S** in Eq. (4),

$$S_{\mathrm{NO_2toNO_x}} = \widetilde{E}_{\mathrm{NO_x}} \frac{\partial C_{\mathrm{NO_2}}}{\partial E_{\mathrm{NO_x}}} = \widetilde{E}_{\mathrm{NO_x}} \frac{\partial C_{\mathrm{NO_2}}}{\partial ((1+x)\widetilde{E}_{\mathrm{NO_x}})} = \frac{\partial C_{\mathrm{NO_2}}}{\partial (1+x)} = \frac{\partial C_{\mathrm{NO_2}}}{\partial x} \tag{9}$$

where $\widetilde{E}$ represents the unperturbed NO_x emission field; x is the perturbation factor. Hence, in this study, the DKF inversion actually seeks the optimal perturbation factor (x) at each iteration. The inversion processes will repeat iteratively until the perturbation factor for each emission region converges within a prescribed criterion, δ (Fig. 2), for which the value of 0.01 was chosen in this study.

2.5 NO_2 observations

2.5.1 Satellite NO_2 measurements

The Dutch–Finnish Ozone Monitoring Instrument (OMI) aboard NASA's EOS Aura satellite, launched on 15 July 2004, is a nadir-viewing UV-Vis spectrometer that measures solar backscattered irradiance in the range of 270 nm to 500 nm. It has been utilized to retrieve atmospheric NO_2 in the spectral range from 405 nm to 465 nm with spatial resolution down to scales of 13 km × 24 km at nadir view point (Levelt et al.,

ACPD
13, 17479–17517, 2013

2006a,b). The EOS Aura satellite follows a Sun-synchronous polar orbit at approximately 705 km altitude with local equator crossing time around 13:40 LT (Levelt et al., 2006b; Boersma et al., 2007). In this study, the NASA standard product, version 2 (Bucsela et al., 2013) retrieval of OMI NO_2, gridded at $0.1^\circ \times 0.1^\circ$ resolution, was obtained from NASA Goddard Space Flight Center and mapped to the 12 km CAMx modeling domain. OMI pixels with cloud radiance fraction greater than 0.5 and sizes of more than 20 km × 63 km at swath edges were excluded in the dataset. The OMI averaging kernels (Eskes and Boersma, 2003) were interpolated into each CAMx model layer and then applied to the modeled NO_2 column density (Eq. 10), to account for the influence of the a priori NO_2 vertical profile used in the OMI retrieval and the OMI measurement sensitivities at each altitude:

$$C_{NO_2}^{modeled} = \sum A_i \cdot X_i \quad (10)$$

where A_i is the averaging kernel at pressure level i, and X_i is the CAMx modeled partial NO_2 subcolumn density at the corresponding pressure level.

In order to reduce the OMI measurement uncertainties and effects from invalid data points, monthly averaged OMI NO_2 column densities were used in the DKF inversions.

2.5.2 Ground and other NO_2 measurements

The US EPA Air Quality System (AQS) NO_2 ground monitoring network data (Fig. 1) (http://www.epa.gov/ttn/airs/airsaqs/) were also used for inverse modeling. AQS monitors are equipped with a heated molybdenum catalytic converter that first transforms NO_2 to NO, and then measures the resultant NO using a chemiluminescence analyzer. NO_2 is then calculated by subtracting NO measured in a separate NO mode from the resultant NO (US EPA, 1975). Studies (US EPA, 1975; Demerjian, 2000; Lamsal et al., 2008) indicate that the catalytic converter also converts fractions of other reactive nitrogen species (e.g. HNO_3, PAN) into NO during this measurement. Therefore, correction factors computed from CAMx modeled concentrations by the method

ACPD
13, 17479–17517, 2013

of Lamsal et al. (2008) (Eq. 11) are applied before deploying the AQS NO_2 data in the DKF inversion:

$$CF = \frac{NO_2}{NO_2 + \sum AN + (0.95PAN) + (0.35HNO_3)} \quad (11)$$

In Eq. (11), $\sum AN$ represents the sum of all alkyl nitrates and PAN is peroxyacetyl nitrate. The CAMx model with CB05 mechanism does not output alkyl nitrates specifically, so the difference between modeled total organic nitrates and PAN was used to represent modeled alkyl nitrates.

The NOAA P-3 aircraft NO_2 data (http://www.esrl.noaa.gov/csd/tropchem/2006TexAQS/) and the Texas Radical and Aerosol Measurement Program (TRAMP) NO_2 data, measured at Moody Tower (Fig. 1), (http://geossun2.geosc.uh.edu/web/blefer/TRAMP/Final%20data/) were used to evaluate the inverse modeling results. The Moody Tower measurement site located at the University of Houston campus is approximately 70 m above the ground (Luke et al., 2010), corresponding to the CAMx modeling layer 2, with hourly NO_2 data available for the whole August–September episode, but no coverage for the June episode. The P-3 aircraft measurement was made from ground level to around 5000 m height with 1 s resolution, but only available on 4 days (31 August, 11 September, 13 September, and 15 September 2006) during our modeling period. Hourly averaged aircraft NO_2 data was used to compare with the hourly modeled NO_2 at corresponding grid cells. Both P-3 aircraft and Moody Tower NO_2 measurements were made by using a photolytic converter, and hence did not require corrections via Eq. (11).

ACPD
13, 17479–17517, 2013

3 Results and discussion

3.1 Pseudodata test for the DKF inversion with CAMx-DDM

To evaluate the performance of the DKF inversion technique, a controlled pseudodata test was performed for 10 modeling days (31 May to 9 June, and 13 August to 22 August) for each modeling episode. The 10 day averaged modeled NO_2 columns at 1–2 p.m. from the base case were used as pseudo-observations, and the model was rerun with NO_x emissions from each region perturbed by known factors ranging from 0.5 to 2.0 (Table 1). Appling the DKF inversion successfully adjusted the perturbed NO_x emissions from each region back to their base values, converging in 4 iterations (Fig. 3). The robustness of the DKF inversion was tested by varying the uncertainty parameters, which were set to 2.0 for emissions and 0.3 for observations in the initial pseudodata test. While higher levels of the emission uncertainty parameter and lower levels of the observation uncertainty parameter led to more rapid adjustments, the final results of the DKF inversion were insensitive to the assumed uncertainty parameters, and also to the off-diagonal elements in the error covariance matrix.

3.2 Additional NO_x emissions

Since DKF inversions scale emissions from their original levels, an appropriate a priori NO_x emission inventory is essential for obtaining reasonable results. The NASA Intercontinental Chemical Transport Experiment (INTEX-A) air quality study (Singh et al., 2006) found large discrepancies between aircraft measurements and CMAQ simulations of NO_2 concentrations in the upper troposphere. Possible explanations could be upper tropospheric NO_x sources such as lightning and aircraft NO_x emissions that are often neglected in emission inventories. Missing NO_x sources in the upper troposphere may bias the inversion on the remaining emissions (Napelenok et al., 2008). At ground level, Hudman et al. (2010) found that the soil NO_x emissions estimated by the widely used Yienger and Levy method (Yienger and Levy, 1995) were underestimated

ACPD
13, 17479–17517, 2013

by a factor of 2 over the United States. Therefore, in this study, the lightning and aircraft NO_x emissions were added in the upper troposphere as described in the Sect. 2.2, and the soil NO_x emissions were doubled from base case levels. The emission inventory with added lightning and aircraft NO_x, and doubled soil NO_x (hereafter referred to as the a priori emission inventory) was used for the following inversion studies. Inclusion of these NO_x sources improves the performance of the model in simulating satellite observed NO_2 column densities, especially in the rural areas (Figs. 4c and 5c), and reduces the bias and error by around 15 % (Table 3).

3.3 Top–down NO_x emissions using OMI NO_2

3.3.1 DS inversion

The DS inversion method was performed with OMI NO_2 column densities to create top-down NO_x emissions for the 12 km modeling domain. The monthly averaged (3 June to 1 July, and 16 August to 15 September) NO_2 column densities at 1–2 p.m. were used to calculate the ratio of OMI to CAMx (Eq. 1). The first three modeling days were discarded for both modeling episodes to avoid the influence of initial conditions. The monthly 24 h averaged NO_x emissions and modeled NO_2 column densities were used to determine the value of the smoothing parameter, k. In this case, k equals to 2.0 for both episodes, indicating large influence of NO_x emissions transported from surrounding grid cells.

Results (Table 2) show the DS inversion scales up the NO_x emissions in all seven regions, leading to higher estimates of modeled NO_2 column densities (Figs. 4d and 5d) in most of the domain. However, especially in urban areas, the simulated NO_2 column densities with inverted NO_x emissions overshoot those observed by OMI. This indicates that the ability of NO_x to influence its own lifetime via changes in OH radical concentrations results in significant nonlinearity between NO_2 concentration and NO_x emission that are neglected by the DS method. Use of inverted NO_x emissions does reduce bias and error in simulating OMI observed column densities, while R^2 gets worse

ACPD
13, 17479–17517, 2013

(Table 3), indicating no improvement in the spatial distribution. The comparisons with AQS ground measurements (Table 4) indicate that the inverted NO_x emissions actually deteriorate the simulations of ground-level NO_2, with bias and error increasing by 70 %. Similar results are shown in evaluating model performance against Moody Tower and P-3 measurements: the DS inversion increases bias and error by approximately 30 % and 20 %, respectively.

3.3.2 DKF inversion

DKF inversion using the OMI NO_2 measurements was conducted to constrain NO_x emissions from the seven designated regions. The monthly averaged (3 June to 1 July, and 16 August to 15 September) OMI and CAMx NO_2 column densities at 1–2 p.m. were used in the inversion. All modeling grids in the inversion area were covered by the OMI NO_2 measurement data. The DKF inversions were performed with 2116 data points in one time step (1–2 p.m.). The scaling factors generated by inversion for each region were applied to the NO_x emission inventory hourly, since we assume that the 1–2 p.m. NO_2 column density is contributed by the NO_x emissions from all previous hours, and the uncertainty in the bottom-up NO_x emission inventory should be the same for every time step. The satellite-based DKF inversions scale a priori NO_x emissions by factors ranging from 1.02 to 1.84 in almost all regions in both episodes (Table 2), adhering to the specified uncertainty range of 0.5 to 2.0. The scaling factors tend to be larger over the rural and small urban regions than over the urban DFW and HGB ozone nonattainment regions, where the inversions scale up emissions only slightly (factors of 1.02 to 1.14). It results from the inversion attempts to compensate for the large gap between higher observed than modeled NO_2 over rural regions, despite varied patterns over urban grid cells. One exception occurs in the NE Texas region in the August–September episode (Table 2), which shows downward scaling (factor of 0.56). This reflects the inversion shifting emissions between NE Texas and the much larger surrounding N rural region (Fig. 1); taken together, the net scaling factor for the two regions in August–September is 1.72, consistent with the upward scaling of rural emis-

ACPD
13, 17479–17517, 2013

sions throughout the two episodes. Apart from this anomaly, scaling factors for most regions were consistent across the two episodes, varying by less than 15 %.

CAMx modeled NO_2 column densities with the inverted NO_x emissions (Figs. 4e and 5e) are increased by 3–55 % in all regions, but the increments are much more moderate compared to the DS method inversion. The statistical results (Table 3) indicate that the DKF inversed NO_2 are closer to OMI observations than the a priori case in terms of 20 % less in bias and 10 % less in error, but without improvements in the spatial distribution. The DS method scales up NO_x emissions more than the DKF inversion (Table 2), making the inversed NO_2 concentrations have slightly less bias and error (Table 3). However, the DKF inversed NO_2 has better R^2 than that of inversed by the DS method, indicating the DKF inversion method has better ability to retain the spatial structure of NO_x emissions. Each of the inversions using OMI NO_2 data actually worsens the model performance in simulating ground level NO_2 concentrations (Table 4), since the modeled ground NO_2 using the base case emission inventory had already been overestimated (Fig. 6). However, the DKF inversed NO_2 only increases the bias and error by 30 % in simulating AQS NO_2 (Table 4), by 5 % in simulating P-3 NO_2 (Table 5), and by 8 % in simulating Moody Tower NO_2, whereas greater deterioration resulted from the DS inversion.

3.4 Top–down NO_x emissions using ground AQS NO_2

Ground-level AQS NO_2 measurements were also used to drive DKF inversions of NO_x emissions for the two modeling episodes. There are 37 ground measurement sites in the designated inversion regions (Fig. 1), mostly located in the urban cores. The N rural and S rural regions were excluded in this case because they contain too few measurement sites. Correction factors from Eq. (11) were applied to the ground NO_2 before using the data in the inversion.

The base case simulations strongly overpredicted observed NO_2 in the early morning and late afternoon during both modeling episodes (Fig. 6), when the model may underestimate planetary boundary layer (PBL) heights (Kolling et al., 2013). To allevi-

ACPD
13, 17479–17517, 2013

ate the influence from PBL heights, daily 24 h averaged NO_2 levels were used in the inversions.

To address the overprediction of ground-level NO_2, the ground-based inversions sharply reduce a priori NO_x emissions by applying scaling factors of 0.30 to 0.57 (Table 2). The reductions in NO_x emissions reduce model error relative to the AQS (Table 4) and Moody Tower NO_2 observations on an hourly basis, as well as NO_2 observed by the P-3 aircraft (Table 5), but may be too sharp, as they lead negative bias in predicting NO_2 from the AQS monitors (Table 4) and the P-3 aircraft measurements (Table 5). More moderate scaling factors are obtained if the inversion is conducted with data only from a midday window (9 a.m.–2 p.m.) when PBL heights are less problematic (not shown). However, scaling factors still remain far below 1.0 and show up to factor of two inconsistencies between the two episodes.

3.5 Impacts on O_3 simulations

O_3 concentrations and their sensitivities to changes in emissions are calculated for both modeling episodes using the a priori and each of the a posteriori emission inventories. The scaled up NO_x emissions from the satellite-based DKF inversion (Table 2) lead to 1–7 ppb higher modeled 8 h (10 a.m.–6 p.m.) O_3 concentrations over most of the domain in the June episode (Fig. 7, top row). Largest increases occur over NE Texas and N rural regions (Fig. 1), where the a priori simulation shows O_3 to be most sensitive to NO_x (Fig. 7, middle row) and where the satellite-based DKF inversion scaled up emissions by large amounts.

The a priori simulation shows O_3 to be primarily sensitive to NO_x over most of the domain, but VOC-limited in the core of the Houston region and with joint sensitivity to NO_x and VOC in Dallas, Austin, and San Antonio (Fig. 7, left column). The satellite-based inversion increases NO_x emissions and thus shifts the O_3 formation chemistry toward being more VOC sensitive (Fig. 7, middle column). Over much of the domain, O_3 sensitivity to VOC increases by a factor of about 1.5. The slight increases in O_3 sensitivity to NO_x occur because the semi-normalized sensitivity coefficients represent the

ACPD
13, 17479–17517, 2013

local slope of O_3-emissions response scaled to a 100 % change in emissions. As the satellite-based inversion scales up NO_x emissions, these semi-normalized coefficients increase, even though the impacts per ton of NO_x decrease.

The ground-based DKF inversion leads to O_3 reductions of 3–8 ppb over urban regions (Fig. 7, top right), where it scales down emissions (Table 2), and less changes over rural regions where emissions were left unchanged due to lack of NO_2 monitors. The reduction in urban NO_x makes O_3 less sensitive to VOC emissions as expected (Fig. 7, bottom right). However, the impact on sensitivity to NO_x is mixed. In urban areas which are transitional between NO_x-limited and NO_x-saturated conditions, the reduction in NO_x emissions pushes the chemistry toward more NO_x-limited conditions and thus increases the sensitivities. In downwind regions which are already NO_x-limited, the sensitivities decline because there are now less NO_x emissions contributing to the semi-normalized coefficients.

Model performance in simulating hourly AQS ground-level observations of O_3 indicates that the bias and error slightly worsened when each of the a posteriori inventories are used in place of the a priori inventory (Table 6). The largest deterioration comes from the DS inversion as the bias and error increase by around 10 %, likely because this inversion method does not retain the spatial structure of emissions from the a priori inventory. For the other inversions, the changes in bias and error are too slight to determine if performance is meaningfully impacted.

4 Conclusions

Inverse modeling has been performed using either NO_2 column densities observed by OMI satellite or ground-level NO_2 concentrations observed by AQS monitors to constrain the NO_x emissions for two regulatory attainment modeling episodes in Texas. Two inversion methods, DS and DKF, are applied to the OMI NO_2 data, and the DKF method is also applied to the ground-level NO_2 data. Pseudodata test results validate that the DKF method effectively captures known perturbations in CAMx simulations.

ACPD
13, 17479–17517, 2013

Two missing NO_x sources in the upper troposphere, lightning and aircraft NO_x emissions, are added into the base case NO_x emission inventory, contributing 14 % and 6 % to the total NO_x emissions for the June episode, and 7 % and 6 % for the August–September episode, respectively. The underestimated soil NO_x emissions are doubled from the base case, adding an additional 8 % NO_x emission to the base case for both episodes. The additional NO_x emissions increase the modeled NO_2 column densities mostly at rural areas and improve the inversion performance with the OMI NO_2, but not with the ground NO_2.

The DS inversions tend to overshoot the OMI-observed NO_2 column densities since this linear inversion method ignores the nonlinear influence of NO_x on its own lifetime. The iterative approach of the DKF inversion avoids this problem, but fails to substantially improve the spatial correlation of modeled and observed NO_2 levels since it applies only a single scaling factor to each inversion region.

The overall tendency of the model to underpredict OMI observed NO_2 column densities and to overpredict AQS observed ground NO_2 concentrations leads to conflicting results between the inversions. It is difficult to determine which observations provide a more reliable basis for the inversions, since none of the inversions improve model performance against independent data such as aircraft-observed NO_2 or ground-level O_3 concentrations. Whether this indicates that the a priori inventory is the best available representation of NO_x emissions, or that tuning of the base model led to its better performance, is impossible to determine. Nevertheless, this suggests that inverse modeling of NO_x emissions should for now remain a complement to SIP modeling efforts rather than a substitute for traditional bottom-up inventories.

The AQS ground NO_2 measurements face limitations due to the inaccuracies of the molybdenum converter method, and because the mostly urban measurement sites may be unrepresentative of the entire region. In addition, model shortcomings in simulating PBL heights may strongly bias the inversions based on ground-level observations.

For the satellite data, several factors could explain the more spatially smeared and higher rural NO_2 in the satellite observations than the base model which drove the up-

ACPD
13, 17479–17517, 2013

ward scaling of emissions. Our inclusion of lightning and aircraft NO_x emissions and doubling of soil NO_x emissions narrowed but did not eliminate the discrepancy. A higher resolution OMI NO_2 product (retrieved with small pixels and high resolution a priori profile) has been shown to enhance NO_2 column densities in urban areas and reduce them in rural areas (Russell et al., 2011), which would more closely resemble the modeled distribution. Lin et al. (2012) highlighted several uncertain model parameterizations that impact model predictions of NO_2 column density for a given emissions inventory. For example, lowering the rate constant of the NO_2 + OH reaction to match the rate of Mollner et al. (2010) would lead to a longer NO_x lifetime and reduce the gap between modeled urban and rural NO_2 concentrations. Henderson et al. (2011) suggested that better representation of acetone and organic nitrates in the CB05 mechanism could help address its underprediction of NO_2 in the remote upper troposphere. Future work could explore how combinations of these adjustments influence satellite-based inversions.

The upcoming DISCOVER-AQ campaign by NASA in fall 2013 will provide vertically resolved measurements of NO_x from repeated aircraft spirals in the Houston region. This may help resolve some of the discrepancies noted here between inversions driven by ground-based and satellite-based NO_2 observations. The future Tropospheric Emissions: Monitoring of Pollution (TEMPO) mission, using a geostationary satellite with high spatial and temporal measurement capabilities, could provide a richer data source to drive the NO_x inversions. Future work could also conduct inversions based on emission categories rather than emission regions, to explore potential errors in the emission inventory on a component rather than location basis.

Acknowledgements. Funding for this research was provided by US National Aeronautics and Space Administration Research Opportunities in Space and Earth Sciences (ROSES) grant NNX10AO05G and by the NASA Air Quality Applied Science Team. The authors thank Jim McKay and Doug Boyer at TCEQ for providing emission inputs, Gary Wilson and Greg Yarwood at ENVIRON for CAMx support, and Tom Ryerson and Winston Luke at NOAA for the P-3 aircraft NO_2 and the Moody Tower NO_2 measurement data.

ACPD
13, 17479–17517, 2013

References

Boersma, K. F., Eskes, H. J., Veefkind, J. P., Brinksma, E. J., van der A, R. J., Sneep, M., van den Oord, G. H. J., Levelt, P. F., Stammes, P., Gleason, J. F., and Bucsela, E. J.: Near-real time retrieval of tropospheric NO_2 from OMI, Atmos. Chem. Phys., 7, 2103–2118, doi:10.5194/acp-7-2103-2007, 2007.

Boersma, K. F., Jacob, D. J., Bucsela, E. J., Perring, A. E., Dirksen, R., van der A, R. J., Yantosca, R. M., Park, R. J., Wenig, M. O., Bertram, T. H., and Cohen, R. C.: Validation of OMI tropospheric NO_2 observations during INTEX-B and application to constrain NO_x emissions over the eastern United States and Mexico, Atmos. Environ., 42, 4480–4497, 2008.

Bovensmann, H., Burrows, J. P., Buchwitz, M., Frerick, J., Noël, S., Rozanov, V. V., Chance, K. V., and Goede, A. P. H.: SCIAMACHY: mission objectives and measurement modes, J. Atmos. Sci., 56, 127–150, 1999.

Brioude, J., Kim, S. W., Angevine, W. M., Frost, G. J., Lee, S. H., McKeen, S. A., Trainer, M., Fehsenfeld, F. C., Holloway, J. S., Ryerson, T. B., Williams, E. J., Petron, G., and Fast, J. D.: Top-down estimate of anthropogenic emission inventories and their interannual variability in Houston using a mesoscale inverse modeling technique, J. Geophys. Res., 116, D20305, doi:10.1029/2011JD016215, 2011.

Bucsela, E. J., Krotkov, N. A., Celarier, E. A., Lamsal, L. N., Swartz, W. H., Bhartia, P. K., Boersma, K. F., Veefkind, J. P., Gleason, J. F., and Pickering, K. E.: A new stratospheric and tropospheric NO_2 retrieval algorithm for nadir-viewing satellite instruments: applications to OMI, Atmos. Meas. Tech. Discuss., 6, 1361–1407, doi:10.5194/amtd-6-1361-2013, 2013.

Chai, T., Carmichael, G. R., Tang, Y., Sandu, A., Heckel, A., Richter, A., and Burrows, J. P.: Regional NO_x emission inversion through a four-dimensional variational approach using SCIAMACHY tropospheric NO_2 column observations, Atmos. Environ., 43, 5046–5055, 2009.

Chang, M. E., Hartley, D. E., Cardelino, C., and Chang, W. L.: Inverse modeling of biogenic isoprene emissions, Geophys. Res. Lett., 23, 3007–3010, 1996.

Deguillaume, L., Beekmann, M., and Menut, L.: Bayesian Monte Carlo analysis applied to regional-scale inverse emission modeling for reactive trace gases, J. Geophys. Res., 112, D02307, doi:10.1029/2006JD007518, 2007.

Demerjian, K. L.: A review of national monitoring networks in North America, Atmos. Environ., 34, 1861–1884, 2000.

ACPD
13, 17479–17517, 2013

ENVIRON: User's Guide to Emissions Processor, Version 3, ENVIRON International Corporation, Novato, CA, 2007.
ENVIRON: Boundary Conditions and Fire Emissions Modeling, Final Report to the Texas Commission on Environmental Quality, ENVIRON International Corporation, Novato, CA, 2008.
ENVIRON: CAMx Users' Guide, version 5.30, ENVIRON International Corporation, Novato, CA, 2010.
Eskes, H. J. and Boersma, K. F.: Averaging kernels for DOAS total-column satellite retrievals, Atmos. Chem. Phys., 3, 1285–1291, doi:10.5194/acp-3-1285-2003, 2003.
Gilliland, A. B. and Abbitt, P. J.: A sensitivity study of the discrete Kalman filter (DKF) to initial condition discrepancies, J. Geophys. Res., 106, 17939–17952, 2001.
Gilliland, A. B., Dennis, R. L., Roselle, S. J., and Pierce, T. E.: Seasonal NH_3 emission estimates for the eastern United States based on ammonium wet concentrations and an inverse modeling method, J. Geophys. Res., 108, 4477, doi:10.1029/2002JD003063, 2003.
Gonzales, M. and Williamson, W.: Updates on the National Ambient Air Quality Standards and the State Implementation Plans for Texas, presented at TCEQ Trade Fair, TX, May 2011.
Grell, G. A., Dudhia, J., and Stauffer, D.: A description of the fifth-generation PennState/NCAR mesoscale model (MM5), NCAR Technical Note, NCAR/TN 398+SR, 1994.
Haas-Laursen, D. E., Hartley, D. E., and Prinn, R. G.: Optimizing an inverse method to deduce time-varying emissions of trace gases, J. Geophys. Res., 101, 22823–22831, 1996.
Hanna, S. R., Lu, Z., Frey, H. C., Wheeler, N., Vukovich, J., Arumachalam, S., and Fernau, M.: Uncertainties in predicted ozone concentration due to input uncertainties for the UAM-V photochemical grid model applied to the July 1995 OTAG domain, Atmos. Environ., 35, 891–903, 2001.
Henderson, B. H., Pinder, R. W., Crooks, J., Cohen, R. C., Hutzell, W. T., Sarwar, G., Goliff, W. S., Stockwell, W. R., Fahr, A., Mathur, R., Carlton, A. G., and Vizuete, W.: Evaluation of simulated photochemical partitioning of oxidized nitrogen in the upper troposphere, Atmos. Chem. Phys., 11, 275–291, doi:10.5194/acp-11-275-2011, 2011.
Hudman, R. C., Russell, A. R., Valin, L. C., and Cohen, R. C.: Interannual variability in soil nitric oxide emissions over the United States as viewed from space, Atmos. Chem. Phys., 10, 9943–9952, doi:10.5194/acp-10-9943-2010, 2010.
Jaeglé, L., Steinberger, L., Martin, R. V., and Chance, K.: Global partitioning of NO_x sources using satellite observations: relative roles of fossil fuel combustion, biomass burning and soil emissions, Faraday Discuss., 130, 407–423, 2005.

ACPD
13, 17479–17517, 2013

Kaynak, B., Hu, Y., Martin, R. V., Russell, A. G., Choi, Y., and Wang, Y.: The effect of lightning NO_x production on surface ozone in the continental United States, Atmos. Chem. Phys., 8, 5151–5159, doi:10.5194/acp-8-5151-2008, 2008.

Kolling, J. S., Pleim, J. E., Jeffries, H. E., and Vizuete, W.: A multisensor evaluation of the Asymmetric Convective Model, Version 2, in Southeast Texas, J. Air Waste Manage., 63, 41–53, doi:10.1080/10962247.2012.732019, 2013.

Konovalov, I. B., Beekmann, M., Richter, A., and Burrows, J. P.: Inverse modelling of the spatial distribution of NO_x emissions on a continental scale using satellite data, Atmos. Chem. Phys., 6, 1747–1770, doi:10.5194/acp-6-1747-2006, 2006.

Konovalov, I. B., Beekmann, M., Burrows, J. P., and Richter, A.: Satellite measurement based estimates of decadal changes in European nitrogen oxides emissions, Atmos. Chem. Phys., 8, 2623–2641, doi:10.5194/acp-8-2623-2008, 2008.

Koo, B., Yarwood, G., and Cohan, D. S.: Incorporation of High-order Decoupled Direct Method (HDDM) Sensitivity Analysis Capability into CAMx; Prepared for Texas Commission on Environmental Quality, 2007.

Koo, B., Chien, C.-J., Tonnesen, G., Morris, R., Johnson, J., Sakulyanontvittaya, T., Piyachaturawat, P., and Yarwood, G.: Natural emissions for regional modeling of background ozone and particulate matter and impacts on emissions control strategies, Atmos. Environ., 44, 2372–2382, 2010.

Koshak, W. J., Solakiewicz, R. J., Blakeslee, R. J., Goodman, S. J., Christian, H. J., Hall, J. M., Bailey, J. C., Krider, E. P., Bateman, M. G., Boccippio, D. J., Mach, D. M., McCaul, E. W., Stewart, M. F., Buechler, D. E., Petersen, W. A., and Cecil, D. J.: North Alabama Lightning Mapping Array (LMA): VHF source retrieval algorithm and error analyses, J. Atmos. Ocean. Tech., 21, 543–558, 2004.

Kurokawa, J., Yumimoto, K., Uno, I., and Ohara, T.: Adjoint inverse modeling of NO_x emissions over eastern China using satellite observations of NO_2 vertical column densities, Atmos. Environ., 43, 1878–1887, 2009.

Lamsal, L. N., Martin, R. V., van Donkelaar, A., Steinbacher, M., Celarier, E. A., Bucsela, E., Dunlea, E. J., and Pinto, J. P.: Ground level nitrogen dioxide concentrations inferred from the satellite borne Ozone Monitoring Instrument, J. Geophys. Res., 113, D16308, doi:10.1029/2007JD009235, 2008.

Lamsal, L. N., Martin, R. V., van Donkelaar, A., Celarier, E. A., Bucsela, E. J., Boersma, K. F., Dirksen, R., Luo, C., and Wang. Y.: Indirect validation of tropospheric nitrogen dioxide re-

ACPD
13, 17479–17517, 2013

trieved from the OMI satellite instrument: insight into the seasonal variation of nitrogen oxides at northern midlatitudes, J. Geophys. Res., 115, D05302, doi:10.1029/2009JD013351, 2010.

Levelt, P. F., Hilsenrath, E., Leppelmeier, G. W., van den Oord, G. H. J., Bhartia, P. K., Tamminen, J., de Haan, J. F., and Veefkind, J. P.: Science objective of the Ozone Monitoring Instrument, IEEE T. Geosci. Remote, 44, 1199–1208, 2006a.

Levelt, P. F., van den Oord, G. H. J., Dobber, M. R., Malkki, A., Visser, H., de Vries, J., Stammes, P., Lundell, J. O. V., and Saari, H.: The Ozone Monitoring Instrument, IEEE T. Geosci. Remote, 44, 1093–1101, 2006b.

Lin, J.-T., McElroy, M. B., and Boersma, K. F.: Constraint of anthropogenic NO_x emissions in China from different sectors: a new methodology using multiple satellite retrievals, Atmos. Chem. Phys., 10, 63–78, doi:10.5194/acp-10-63-2010, 2010.

Lin, J.-T., Liu, Z., Zhang, Q., Liu, H., Mao, J., and Zhuang, G.: Modeling uncertainties for tropospheric nitrogen dioxide columns affecting satellite-based inverse modeling of nitrogen oxides emissions, Atmos. Chem. Phys., 12, 12255–12275, doi:10.5194/acp-12-12255-2012, 2012.

Luke, W. T., Kelley, P., Lefer, B. L., Flynn, J., Rappenglück, B., Leuchner, M., Dibb, J. E., Ziemba, L. D., Anderson, C. H., and Buhr, M.: Measurements of primary trace gases and NO_y composition in Houston, Texas, Atmos. Environ., 44, 4068–4080, 2010.

Martin, R. V., Jacob, D. J., Chance, K., Kurosu, T. P., Palmer, P. I., and Evans, M. J.: Global inventory of nitrogen oxide emissions constrained by space-based observations of NO_2 columns, J. Geophys. Res., 108, 4537, doi:10.1029/2003JD003453, 2003.

Martin, R. V., Sioris, C. E., Chance, K., Ryerson, T. B., Bertram, T. H., Wooldridge, P. J., Cohen, R. C., Neuman, J. A., Swanson, A., and Flocke, F. M.: Evaluation of space-based constraints on global nitrogen oxide emissions with regional aircraft measurements over and downwind of eastern North America, J. Geophys. Res., 111, D15308, doi:10.1029/2005JD006680, 2006.

Mendoza-Dominguez, A. and Russell, A. G.: Iterative inverse modeling and direct sensitivity analysis of a photochemical air quality model, Environ. Sci. Technol., 34, 4974–4981, 2000.

Mollner, A. K., Valluvadasan, S., Feng, L., Sprague, M. K., Okumura, M., Milligan, D. B., Bloss, W. J., Sander, S. P., Martien, P. T., Harley, R. A., McCoy, A. B., and Carter, W. P. L.: Rate of gas phase association of hydroxyl radical and nitrogen dioxide, Science, 330, 646–649, doi:10.1126/science.1193030, 2010.

ACPD
13, 17479–17517, 2013

Mulholland, M. and Seinfeld, J. H.: Inverse air pollution modeling of urban-scale carbon monoxide emissions, Atmos. Environ., 29, 497–516, 1995.
Müller, J.-F. and Stavrakou, T.: Inversion of CO and NO_x emissions using the adjoint of the IMAGES model, Atmos. Chem. Phys., 5, 1157–1186, doi:10.5194/acp-5-1157-2005, 2005.
Napelenok, S. L., Pinder, R. W., Gilliland, A. B., and Martin, R. V.: A method for evaluating spatially-resolved NO_x emissions using Kalman filter inversion, direct sensitivities, and space-based NO_2 observations, Atmos. Chem. Phys., 8, 5603–5614, doi:10.5194/acp-8-5603-2008, 2008.
Pison, I., Menut, L., and Bergametti, G.: Inverse modeling of surface NO_x anthropogenic emission fluxes in the Paris area during the Air Pollution Over Paris Region (ESQUIF) campaign, J. Geophys. Res., 112, D24302, doi:10.1029/2007JD008871, 2007.
Prinn, R. G.: Measurement equation for trace chemicals in fluids and solution of its inverse, in: Inverse Methods in Global Biogeochemical Cycles, vol. 114, edited by: Kasibhatla, P., et al., AGU, Washington, DC, 3–18, 2000.
Quélo, D., Mallet, V., and Sportisse, B.: Inverse modeling of NO_x emissions at regional scale over northern France: preliminary investigation of the second-order sensitivity, J. Geophys. Res., 110, D24310, doi:10.1029/2005JD006151, 2005.
Rodgers, C. D.: Inverse Methods for Atmospheric Sounding Theory and Practice, 1st edn., World Scientific, Singapore, 2000.
Russell, A. R., Perring, A. E., Valin, L. C., Bucsela, E. J., Browne, E. C., Wooldridge, P. J., and Cohen, R. C.: A high spatial resolution retrieval of NO_2 column densities from OMI: method and evaluation, Atmos. Chem. Phys., 11, 8543–8554, doi:10.5194/acp-11-8543-2011, 2011.
Seinfeld, J. H. and Pandis, S. N.: Atmospheric Chemistry and Physics, John Wiley & Sons, New Jersey, 2006.
Singh, H. B., Brune, W. H., Crawford, J. H., Jacob, D. J., and Russell, P. B.: Overview of the summer 2004 intercontinental chemical transport experiment – North America (INTEX-A), J. Geophys. Res., 111, D24S01, doi:10.1029/2006JD007905, 2006.
TCEQ: Houston–Galveston–Brazoria Attainment Demonstration SIP Revision for the 1997 Eight-Hour Ozone Standard, Austin, TX, 2010.
TCEQ: Dallas-Fort Worth Attainment Demonstration SIP Revision for the 1997 Eight-hour Ozone Standard Non-attainment Area, Austin, TX, 2011.
Toenges-Schuller, N., Stein, O., Rohrer, F., Wahner, A., Richter, A., Burrows, J. P., Beirle, S., Wagner, T., Platt, U., and Elvidge, C. D.: Global distribution pattern of anthropogenic nitrogen

ACPD
13, 17479–17517, 2013

oxide emissions: correlation analysis of satellite measurements and model calculations, J. Geophys. Res., 111, D05312, doi:10.1029/2005JD006068, 2006.
Turner, A., Henze, D. K., Martin, R. V., and Hakami, A.: The spatial extent of source influences on modeled column concentrations of short-lived species, Geophys. Res. Lett., 39, L12806, doi:10.1029/2012GL051832, 2012.
US EPA: Technical assistance document for the chemiluminescence measurement of nitrogen dioxide, Tech. Rep., Environmental Monitoring and Support Laboratory, N.C. EPA-600/4-75-003, US EPA, Research Triangle Park, 1975.
US EPA: CFR Title 40: Protection of Environment, Part 58-Ambient Air Quality Surveillance, Washington, DC, 2006.
Welch, G. and Bishop, G.: An introduction to the Kalman Filter, University of North Carolina, Chapel Hill, NC, 2001.
Xiao, X., Cohan, D. S., Byun, D. W., and Ngan, F.: Highly nonlinear ozone formation in the Houston region and implications for emission controls, J. Geophys. Res., 115, D23309, doi:10.1029/2010JD014435, 2010.
Yarwood, G., Wilson, G., Emery, C., and Guenther, A.: Development of the GloBEIS – a state of the science biogenic emissions modeling system, Final Report to the Texas Natural Resource Conservation Commission, Austin, TX, 1999.
Yienger, J. J. and Levy, H.: Empirical-model of global soil-biogenic NO_x emissions, J. Geophys. Res., 100, 11447–11464, doi:10.1029/95JD00370, 1995.
Zhao, C. and Wang, Y.: Assimilated inversion of NO_x emissions over east Asia using OMI NO_2 column measurements, Geophys. Res. Lett., 36, L06805, doi:10.1029/2008GL037123, 2009.

ACPD
13, 17479–17517, 2013

Table 1. Arbitrary perturbation factors for pseudodata testing.

Source Region	Perturbation factor
HGB	1.8
DFW	0.6
BPA	1.6
NE Texas	0.7
Austin and San Antonio	1.4
N rural	1.5
S rural	0.8

ACPD
13, 17479–17517, 2013

Table 2. Scaling factors for each region from different inversions.

Source Region	3 Jun to 1 Jul 2006					16 Aug to 15 Sep 2006				
	Base NO_x emission (td^{-1})	Priori NO_x emission[a] (td^{-1})	Scaling factor relative to priori (unitless)			Base NO_x emission (td^{-1})	Priori NO_x emission (td^{-1})	Scaling factor relative to priori (unitless)		
			Posteriori OMI-based DS inversion	Posteriori OMI-based DKF inversion	Posteriori Ground-based DKF inversion[b]			Posteriori OMI-based DS inversion	Posteriori OMI-based DKF inversion	Posteriori Ground-based DKF inversion
HGB	374	455	1.46	1.12	0.37	382	436	1.56	1.03	0.57
DFW	335	435	1.36	1.02	0.34	314	412	1.47	1.14	0.47
BPA	81	97	2.23	1.83	0.49	86	98	2.02	1.75	0.42
NE Texas	141	164	2.33	1.84	0.49	155	174	1.69	0.56	0.51
Austin and San Antonio	252	319	1.55	1.28	0.30	248	302	1.82	1.70	0.40
N rural	522	823	1.93	1.67	–	543	759	2.00	1.98	–
S rural	472	728	1.83	1.52	–	489	668	2.04	1.72	–

[a] Adds lightning and aircraft NO_x, and doubled soil NO_x emissions to the base case.

[b] Conducted with 24 h averaged ground-level NO_2 data.

ACPD
13, 17479–17517, 2013

Table 3. Performance of CAMx in simulating OMI-observed NO_2 column densities.

Statistical Parameters	3 Jun to 1 Jul 2006				16 Aug to 15 Sep 2006			
	Base case	Priori[c]	Posteriori OMI-based DS inversion	Posteriori OMI-based DKF inversion	Base case	Priori	Posteriori OMI-based DS inversion	Posteriori OMI-based DKF inversion
R^2	0.62	0.61	0.42	0.54	0.63	0.48	0.40	0.51
NMB[a]	−0.47	−0.30	0.087	−0.12	−0.54	−0.33	0.13	−0.12
NME[b]	0.48	0.32	0.22	0.23	0.55	0.39	0.32	0.28

[a] Normalized mean bias.
[b] Normalized mean error.
[c] Adds lightning and aircraft NO_x, and doubled soil NO_x emissions to the base case.

ACPD
13, 17479–17517, 2013

Table 4. Performance of CAMx in simulating AQS Ground-level NO_2[a].

Statistical Parameters	3 Jun to 1 Jul 2006					16 Aug to 15 Sep 2006				
	Base case	Priori	Posteriori OMI-based DS inversion	Posteriori OMI-based DKF inversion	Posteriori Ground-based DKF inversion	Base case	Priori	Posteriori OMI-based DS inversion	Posteriori OMI-based DKF inversion	Posteriori Ground-based DKF inversion
R^2	0.55	0.54	0.49	0.51	0.52	0.50	0.49	0.43	0.44	0.47
NMB	0.82	0.91	1.66	1.30	−0.16	0.35	0.42	1.10	0.72	−0.24
NME	0.96	1.03	1.71	1.37	0.48	0.63	0.67	1.21	0.91	0.48

[a] Hourly AQS data was used to compare with modeled NO_2 at corresponding locations.

ACPD
13, 17479–17517, 2013

Table 5. Performance of CAMx in simulating P-3 aircraft-observed NO_2.

Statistical Parameters	16 Aug to 15 Sep 2006[a]				
	Base case	Priori	Posteriori OMI-based DS inversion	Posteriori OMI-based DKF inversion	Posteriori Ground-based DKF inversion
R^2	0.23	0.23	0.25	0.22	0.22
NMB	0.10	0.10	0.46	0.15	−0.14
NME	0.99	0.99	1.24	1.02	0.86

[a] Comparison available for only four days (31 August, 11 September, 13 September, and 15 September 2006).

ACPD
13, 17479–17517, 2013

Table 6. Performance of CAMx in simulating AQS hourly ground-level O_3.

Statistical Parameters	3 Jun to 1 Jul 2006				16 Aug to 15 Sep 2006			
	Priori	Posteriori OMI-based DS inversion	Posteriori OMI-based DKF inversion	Posteriori Ground-based DKF inversion	Priori	Posteriori OMI-based DS inversion	Posteriori OMI-based DKF inversion	Posteriori Ground-based DKF inversion
R^2	0.61	0.61	0.63	0.58	0.50	0.52	0.51	0.46
NMB	0.01	0.12	0.02	0.04	0.38	0.49	0.41	0.40
NME	0.29	0.37	0.30	0.30	0.47	0.58	0.50	0.48

ACPD
13, 17479–17517, 2013

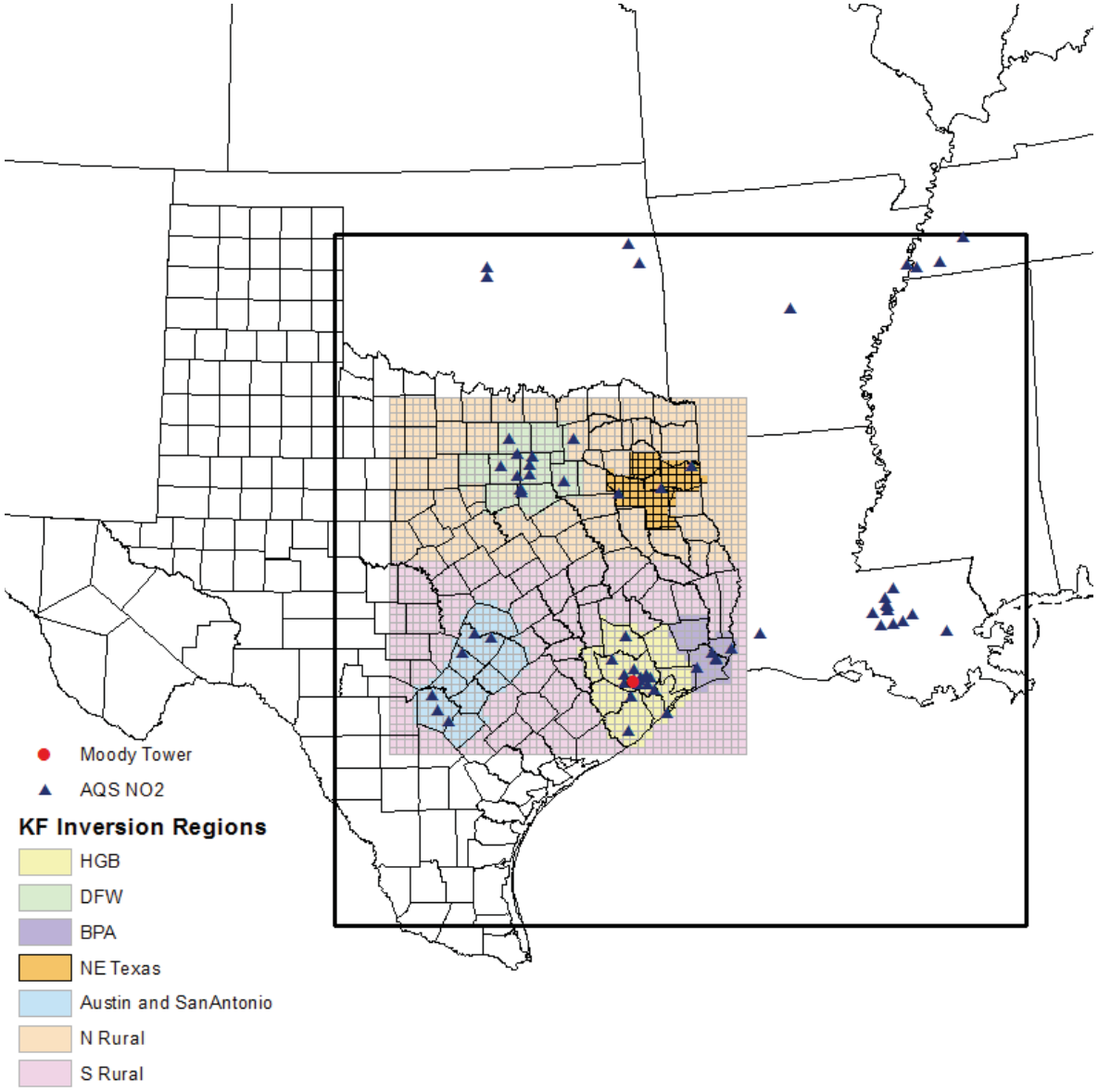

Fig. 1. 12 km CAMx modeling domain for eastern Texas (black square), inversion regions (shaded), ground AQS NO_2 monitoring sites (blue triangles), and Moody Tower (red circle).

ACPD
13, 17479–17517, 2013

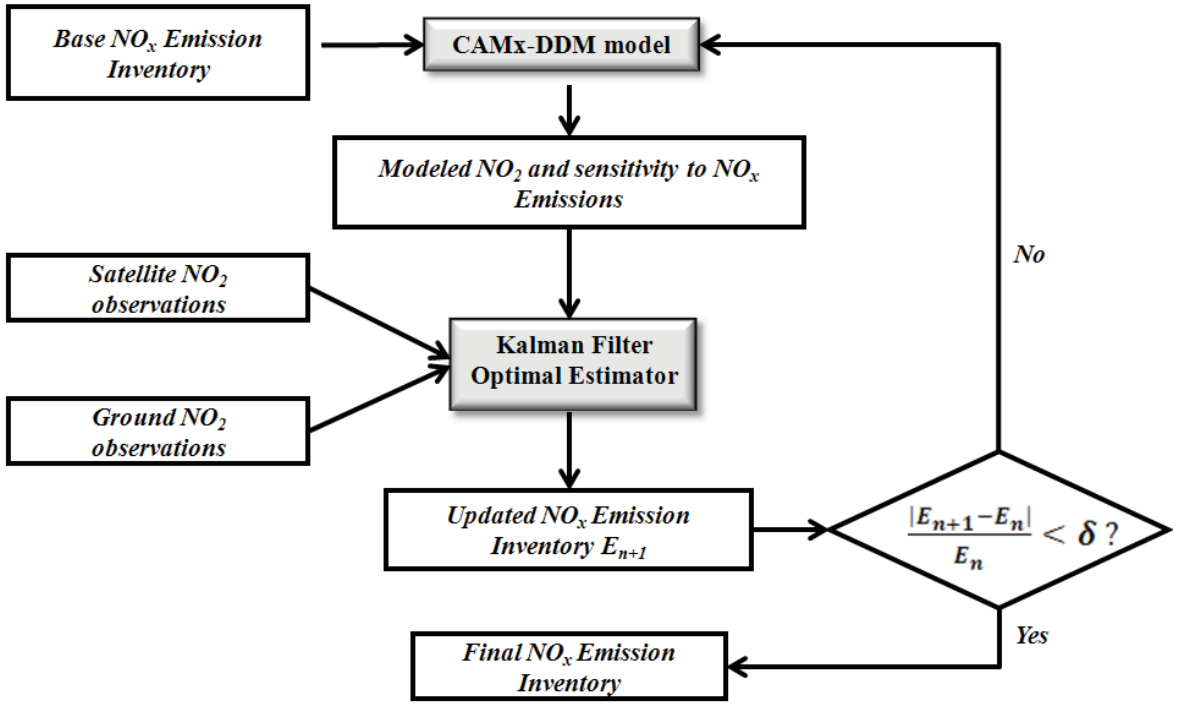

Fig. 2. Schematic diagram of Kalman filter inversion process.

ACPD
13, 17479–17517, 2013

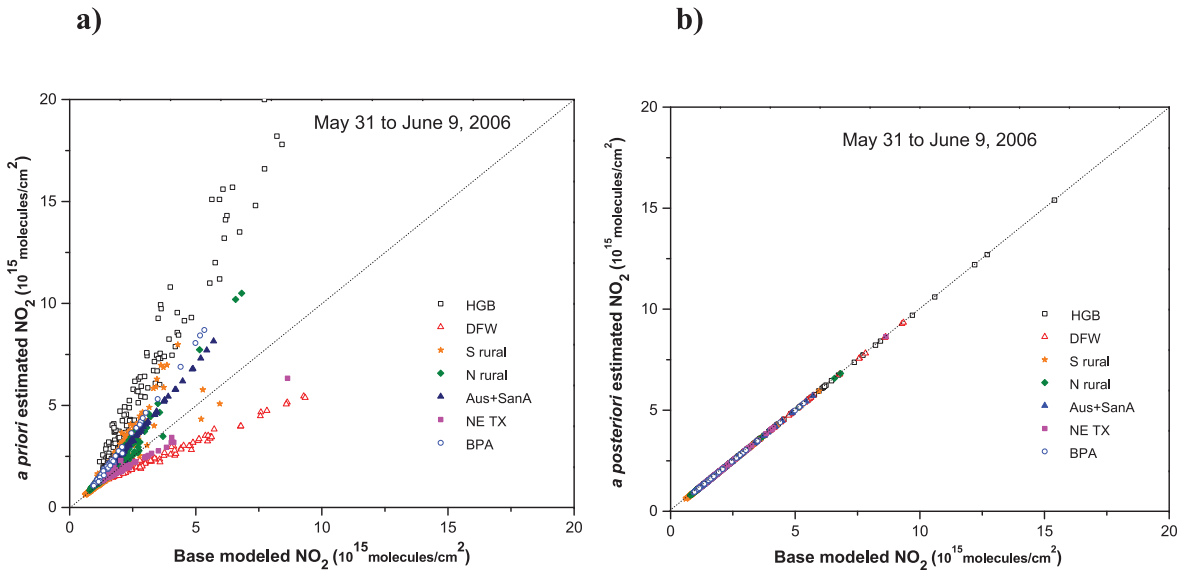

Fig. 3. Pseudodata test showing that the DKF inversion accurately adjusts the NO_x emissions from the perturbed case **(a)** to the a posteriori case **(b)** to match the desired base NO_2 column densities. Similar performance is found for the 13–22 August test period.

ACPD
13, 17479–17517, 2013

Inverse modeling of Texas NO_x emissions

W. Tang et al.

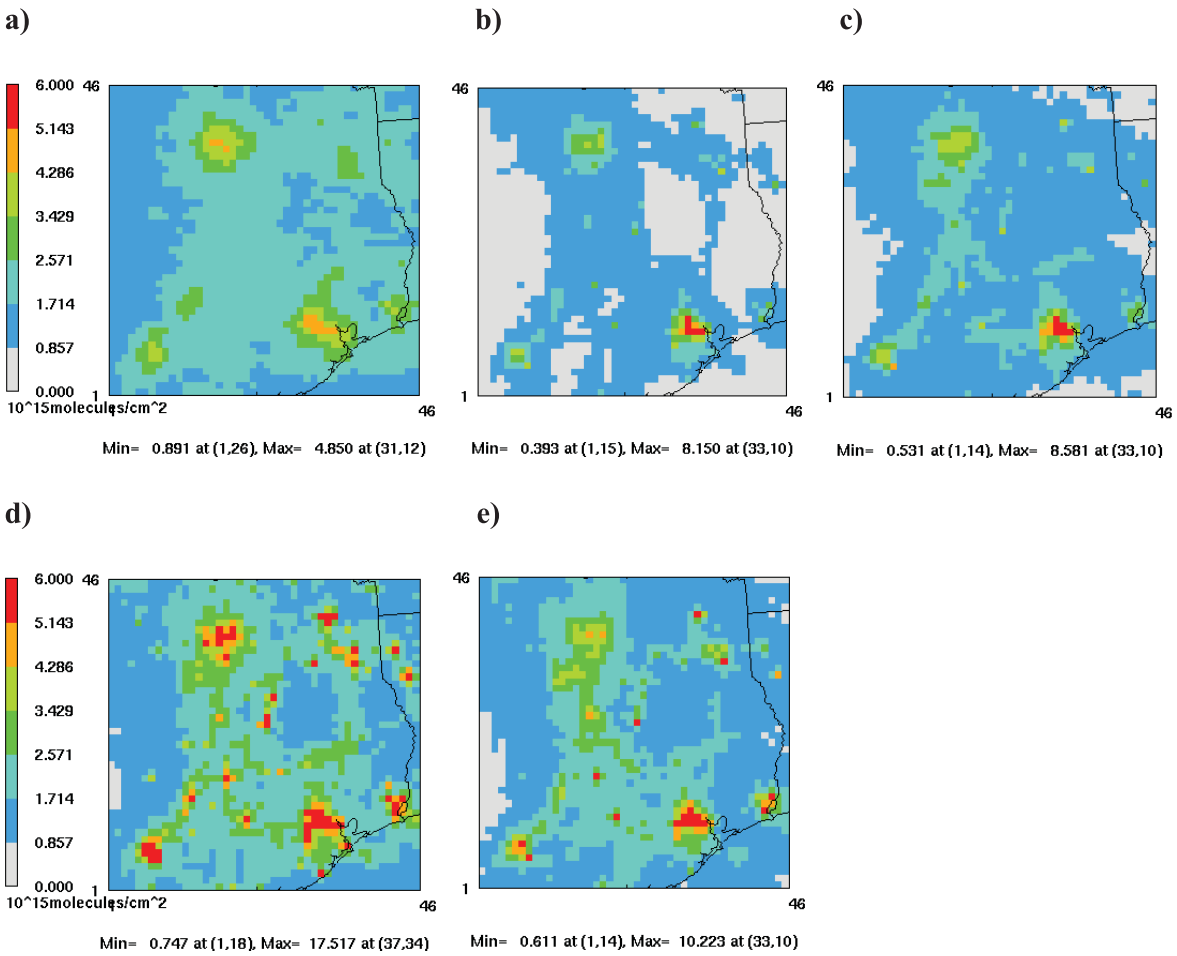

Fig. 4. Monthly averaged (3 June to 1 July) tropospheric NO_2 vertical columns at 1–2 p.m. from **(a)** OMI observations, and from CAMx simulations using **(b)** base case emissions inventory, **(c)** a priori emission inventory (with additional lightning, aircraft, and soil NO_x), and OMI-based inverted NO_x emissions using **(d)** DS and **(e)** DKF methods.

ACPD
13, 17479–17517, 2013

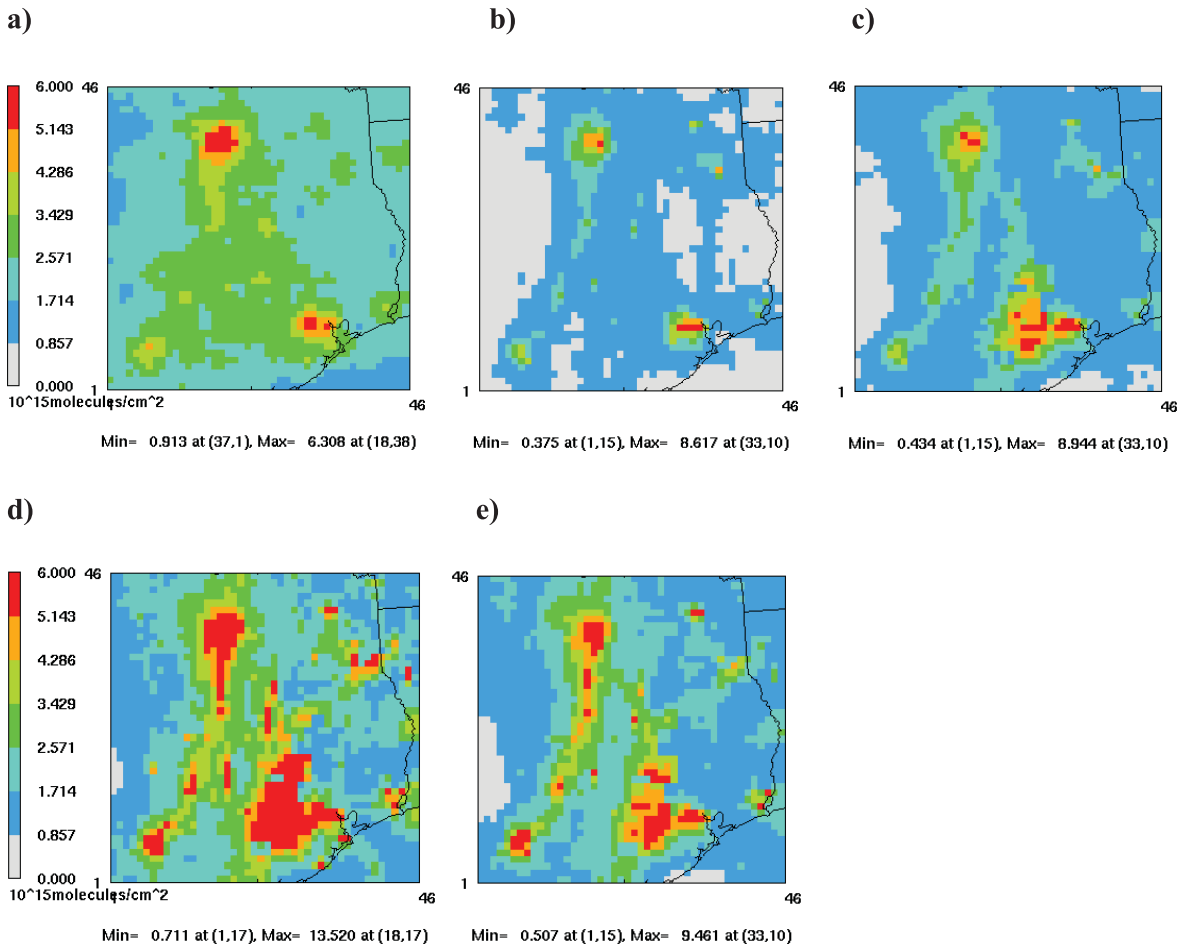

Fig. 5. Same as Fig. 4, but for the August–September episode.

ACPD
13, 17479–17517, 2013

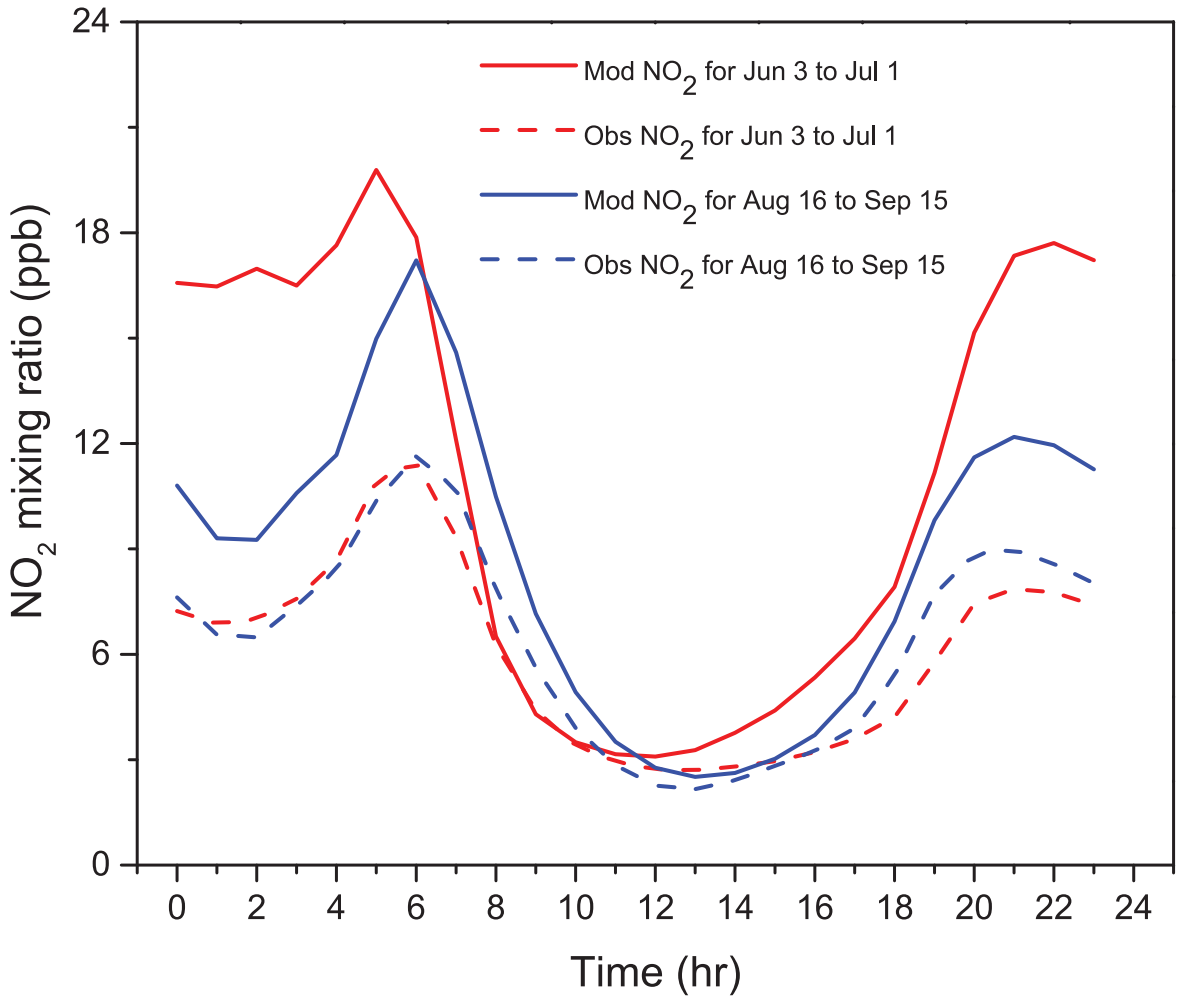

Fig. 6. Daily variations of modeled (solid line) and observed (dashed line) ground NO_2 concentrations for the June (red) and August–September (blue) episodes. Note: NO_2 concentrations were taken by averaging monthly data for all sites.

ACPD
13, 17479–17517, 2013

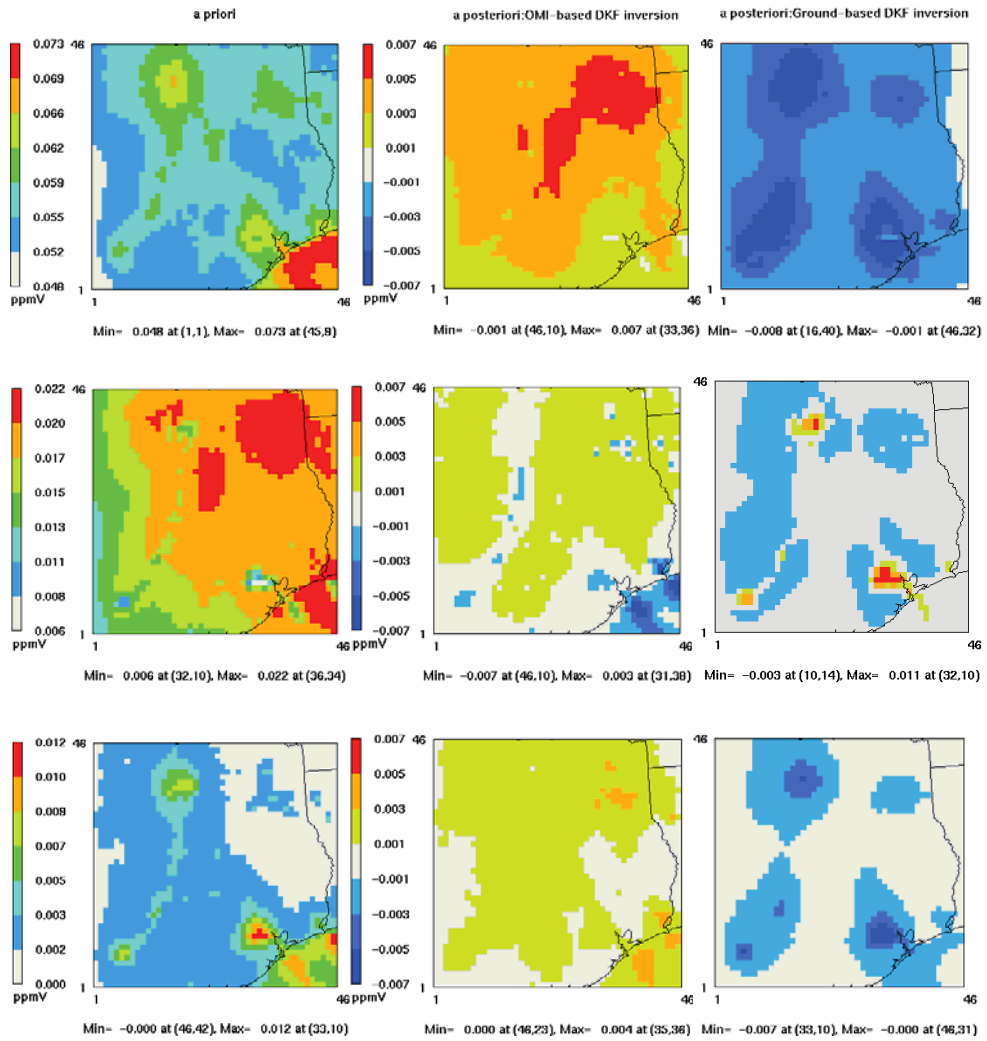

Fig. 7. Monthly 8 h (10 a.m.–6 p.m.) averaged ground-level O_3 concentrations (top), O_3 sensitivity to NO_x (middle), and O_3 sensitivity to VOC (bottom) for the a priori case (left column), and differences (a posteriori minus a priori) for the OMI-based (middle column) and ground-based (right column) DKF inversions in the June episode. The August–September episode shows similar results.

ACPD
13, 17479–17517, 2013

Inverse modeling of Texas NO_x emissions

W. Tang et al.